Using the Back Propagation Neural Network Approach to Bias Correct TMPA Data in the Arid Region of Northwest China

YANFEN YANG

Key Laboratory of Ecosystem Network Observation and Modeling, Institute of Geographic Sciences and Natural Resources Research, Chinese Academy of Sciences, and University of Chinese Academy of Sciences, Beijing, China

YI LUO

Key Laboratory of Ecosystem Network Observation and Modeling, Institute of Geographic Sciences and Natural Resources Research, Chinese Academy of Sciences, Beijing, China

(Manuscript received 2 March 2013, in final form 17 June 2013)

ABSTRACT

Scarcity or unavailability of precipitation observation creates difficulties in hydrologic modeling of mountainous sections of the arid region of northwest China (34°–50°N, 72°–107°E). Tropical Rainfall Measuring Mission (TRMM) precipitation products may be a potential substitute, but they should be evaluated and corrected with ground observation data before application. In this paper, two TRMM Multisatellite Precipitation Analysis (TMPA) precipitation products were evaluated by gauge observations, using indices such as frequency bias index, probability of detection, false alarm ratio, relative mean bias, Nash–Sutcliffe efficiency, and correlation coefficient. Terrain variables were extracted from a digital elevation model, and their rotated principal components were determined to establish a stepwise regression model to adjust TMPA precipitation. Additionally, a back-propagation (BP) neural network was established to correct TMPA precipitation. The results showed that TMPA had an unsatisfactory detection ability in the study area for both precipitation occurrence and amount. TMPA precipitation corrected by a stepwise regression method showed some improvement, but only the results for TRMM 3B43 on a subregion scale were acceptable. The BP neural network method showed better results than the stepwise regression method, and both TRMM 3B42 and TRMM 3B43 corrected by the former method on a subregion scale could be acceptable. Both methods were spatial-scale dependent and showed better results on a subregion scale than on a larger scale.

1. Introduction

Precipitation is a major component of water resources and is of great importance in studying hydrology, meteorology, and agriculture (Li and Shao 2010). The hydrologic cycle begins with the amount of precipitation in one area. Accurate precipitation input is the basic precondition for reliable hydrologic simulation, and precipitation accuracy affects the predictive ability of rainfall–runoff models (Duncan et al. 1993). Precipitation input, which is often more critical to the success of a model application than the choice of hydrologic model complexity (Gan et al. 1997), must therefore be as reliable as possible.

It is generally impracticable to establish a rain gauge network in mountainous regions or remote areas because of the high cost of establishing and maintaining the equipment. These two factors lead to an uneven distribution of gauges, both horizontally and vertically. Furthermore, the catch of conventional rain gauges is only a small radius around the instrument (Collischonn et al. 2008); scarce point observations are often not representative over large regions with complex topography, thereby resulting in unsatisfactory performance of a rainfall–runoff model.

Precipitation products with wide coverage and high temporal–spatial resolution are obtained from analyzing cloud layers by combining geostationary satellite data and low-orbit satellite information (Boushaki et al. 2009) and may be a potential substitute for precipitation data.

Corresponding author address: Yi Luo, Key Laboratory of Ecosystem Network Observation and Modeling, Institute of Geographic Sciences and Natural Resources Research, Chinese Academy of Sciences, 11A, Datun Road, Chaoyang District, Beijing 100101, China.
E-mail: luoyi.cas@hotmail.com

DOI: 10.1175/JHM-D-13-041.1

Examples of such products are Tropical Rainfall Measuring Mission (TRMM; Huffman et al. 2003), Precipitation Estimation from Remotely Sensed Information using Artificial Neural Networks (PERSIANN; Sorooshian et al. 2000), Climate Prediction Center's morphing technique (CMORPH; Joyce et al. 2004), and others. However, satellites observe cloud layers, rather than direct precipitation (Xie and Arkin 1995). Additionally, sampling error (Bowman 2005) and uncertainty of retrieval algorithms (Kummerow 1998) result in error and bias for satellite precipitation observations. Therefore, a series of studies were conducted with focus on quantifying error in satellite precipitation estimates.

Results show that TRMM precipitation is more reliable than other satellite data (Nicholson et al. 2003b). Nevertheless, the performance of the TRMM is critically dependent on the sensor limitation (Huffman and Bolvin 2013), quality of the input datasets, spatial and time scale, precipitation rate (Huffman et al. 2010), and sampling errors (Bowman 2005). Previous studies indicate that TRMM performs differently by region and season (Dinku et al. 2007, 2008; Scheel et al. 2010). TRMM shows better performance over ocean than land because the primary task of TRMM is to measure rainfall in tropical and subtropical regions, and TRMM Microwave Imager (TMI) is less effective over land surfaces because of variations in the surface emissivity (Bowman 2005). Barros et al. (2006) indicate that TRMM has difficulty detecting precipitation in high-altitude areas because there is a strong effect of the relief itself on the microwave signal in mountainous terrain (Mätzler and Standley 2000). Seasonally, TRMM tends to show better performance in warm/convective conditions and vice versa in cool-season stratiform conditions, resulting from infrared (IR) estimates that are better correlated to short-interval precipitation in convective conditions (Ebert et al. 2007; Huffman et al. 2010). More specifically, TRMM shows various performances all over the world. For example, TRMM 3B42 overestimates rainfall over the Zambezi River basin (Cohen Liechti et al. 2012) and the Tibetan Plateau (Yin et al. 2008) and underestimates rainfall on most days in Nepal (Islam 2009). TRMM 3B43 shows excellent agreement with gauge measurements on monthly to seasonal time scales for West Africa (Nicholson et al. 2003b), but there is lower linear correlation for areas around large continental water bodies, such as Lake Issyk-Kul in eastern Kyrgyzstan (Karaseva et al. 2012).

Several methods have been developed to correct satellite precipitation data for practical use. Microwave (MW) and IR sensor data may be merged to increase reliability and accuracy of rainfall estimation in areas with no gauge data (Hong et al. 2007; Joyce et al. 2004), or satellite precipitation and ground-based data may be merged using statistical or regression methods in areas with available rain gauge data (Boushaki et al. 2009; Huffman et al. 2007; Janowiak et al. 2009; Morrissey and Greene 1993; Tian et al. 2010; Tobin and Bennett 2010; Yan and Gebremichael 2009; Yin et al. 2004, 2008). MW gives an accurate instantaneous rain rate, but with poor sampling in space and time. IR estimates have good coverage in space and frequent sampling in time, but with significant systematic errors. Combining MW and IR may compensate for the shortcomings of each, producing more accurate rainfall estimates with wide coverage and high resolution. However, there remains precipitation retrieval algorithm uncertainty in this type of method. Statistical correction approaches, such as adjusting the probability distribution function of satellite rainfall to actual rainfall (Tobin and Bennett 2010) or taking the maximum likelihood value of measured rainfall for given satellite data as the corrected value (Tian et al. 2010), rely on both satellite estimates and rain gauge data. Nevertheless, these methods lack physical meaning because there may be not a simple statistical relationship between the two when considering the impact of terrain on precipitation. The stepwise regression method (Yin et al. 2008) establishes regression models by taking satellite rainfall and terrain variables as independent and rain gauge data as dependent, and these models are used to correct rainfall estimates. Drawbacks remain in this method because terrain variables have complex effects on precipitation, and the regression equations are often linear models that cannot describe these effects well. Therefore, a new method is needed to correct satellite precipitation estimates and achieve higher precision. The method must account for the nonlinear relationship between rain gauge precipitation and terrain variables.

The arid region of northwest China (34°–50°N, 72°–107°E) is extensive and of complex topography. Elevation ranges from −214 to 8366 m MSL. Only 80 rain gauges are available in this large area, with altitudes of the lowest and highest stations at 37.2 and 3507.2 m MSL, respectively. Most gauges are below 2000 m MSL, and there are a few at high elevations above 3510 m MSL. This scarce and uneven distribution of gauges results in very deficient or insufficient representation of precipitation and causes difficulties in hydrologic simulation of this area. Therefore, TRMM products represent a potential substitute for precipitation data. However, the accuracy of TRMM in this area must be evaluated, and precipitation should be corrected for reliable application. Therefore, this paper focuses on 1) evaluating the detection ability of TRMM precipitation product in the arid zone of northwest China and 2) developing a method for correcting TRMM precipitation data with limited rain gauge data.

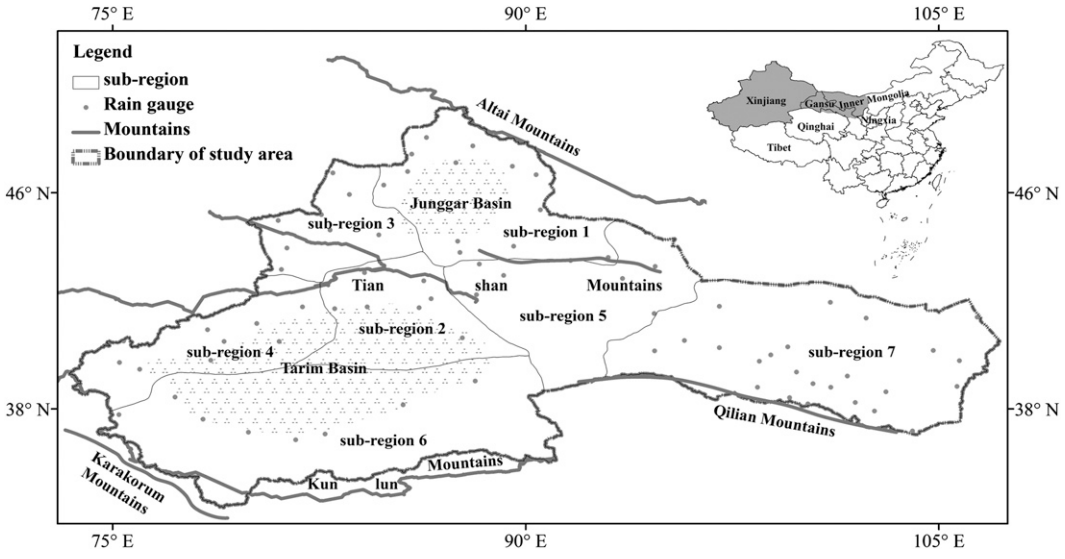

FIG. 1. Study area and locations of rain gauges.

2. Materials and methods

a. Description of study area

The study area has an area of 2.27 million km^2, constituting 23.6% of the total area of China. The area includes Xinjiang province and parts of Gansu, Inner Mongolia, Qinghai, and Ningxia provinces (Fig. 1). The area is characterized by mountains and basins. In Xinjiang, mountains and basins are arranged in a staggered manner, with the Altai Mountains in the north and the Kunlun Mountains in the south. The Tian Shan spans the middle and divides Xinjiang into two parts, southern Xinjiang and northern Xinjiang (Chen et al. 2012; Zhang et al. 2012). These high-elevation mountains block atmospheric circulations and create two vast desert basins in the rain shadows between the mountains. These are the Tarim Basin in the south and Junggar Basin in the north (Shi et al. 2007). Another part of the study area features the Qilian Shan mountain range in Gansu province and the relatively moderate terrain of Inner Mongolia. To analyze the spatial heterogeneity of meteorological factors in the region, Zhao et al. (2011) divided Xinjiang into six subregions. We followed this delineation of subregions in our study, and areas outside Xinjiang province were considered a single subregion (Fig. 1).

As shown in Table 1, a large proportion of the area is located at 500–2000 and 3510–6000 m MSL. There is a typical inland arid climate with unevenly distributed precipitation, most of which falls in the mountains, where long-term average annual precipitation reaches 400 mm or more. Junggar Basin, Gansu, and Inner Mongolia have average annual precipitation from 100 to 200 mm, while Tarim Basin only receives 20–80 mm. This precipitation for the entire study area is less than 200 mm (Su et al. 2007; Zhang et al. 2011).

b. Data sources

1) GROUND DATA

(i) Rain gauge data

Observed daily precipitation of the 80 rain gauges in the region was from the China Meteorological Data Sharing Service System. The precipitation data record is from 1 January 1951 to the present. Four gauges were excluded, owing to their mismatched time span with TRMM data. Daily precipitation data from the remaining 76 gauges were rigorously quality controlled. The gauges are unevenly distributed both vertically and horizontally.

TABLE 1. Distribution of area and number of rain gauges along the elevations of the arid region of northwest China.

Elevation band (m MSL)	Medium elevation (m MSL)	Area (km^2)	Area ratio	No. rain gauges
−214–0	−107	3615	0.002	0
0–500	250	103 764	0.046	6
500–1000	750	442 114	0.195	18
1000–1500	1250	790 371	0.349	29
1500–2000	1750	253 473	0.112	16
2000–2500	2250	117 101	0.052	2
2500–3000	2750	89 997	0.040	1
3000–3510	3255	96 521	0.043	4
3510–6000	4755	366 309	0.162	0
6000–8366	7183	4540	0.002	0
Total		2 267 805	1	76

Most are between 500 and 2000 m MSL, and there are none above 3510 m MSL (Table 1).

(ii) DEM

We also used Advanced Spaceborne Thermal Emission and Reflection Radiometer (ASTER) digital elevation model (DEM) data, with coverage from 83°N to 83°S and resolution of 1 arc s (30-m horizontal spacing at the equator). The data were available from the National Aeronautics and Space Administration (NASA) Warehouse Inventory Search Tool (WIST).

2) TMPA DATA

TRMM is a joint U.S.–Japan satellite mission to monitor tropical and subtropical precipitation. It was launched in late November 1997 into circular orbit, at approximately 350-km altitude (elevated to 420 km in 2001) and 35° inclination from the equatorial plane. The spacecraft takes about 91 min to complete one orbit (Collischonn et al. 2008). The TRMM project provides various products through a combination of different satellite sensors, among which level 3 are gridded precipitation products, including 3A11, 3A25, 3B31, and TMPA (3B42 and 3B43). The first three kinds of products have a resolution of at least 0.5° × 0.5° and have a spatial coverage of 40°N–40°S [see http://mirador.gsfc.nasa.gov/cgi-bin/mirador/presentNavigation.pl?tree=project&project=TRMM&dataGroup=Gridded&CGISESSID=ba7d85e288dffc92426ab7c45d23ca30&location=(-90,-180),(90,180)], which could not meet our needs because the study area covered 34°–50°N. The latest TMPA version 7 products, which have finer resolution of 0.25° × 0.25° and cover 50°N–50°S, were therefore adopted in this study.

c. Data analysis

1) DATA PREPROCESSING

We analyzed precipitation data from 1 January 1998 to 31 December 2010. Daily precipitation from rain gauges and TRMM 3B42 were aggregated to monthly temporal resolution. Point data of observed precipitation were processed by generating a buffer of 25 km in diameter for each rain gauge, matching the 0.25° × 0.25° TMPA pixel data. Precipitation in the buffer is approximately equal to that of gauge data. Universal kriging with a linear drift trend was used to interpolate TMPA precipitation, producing a smooth precipitation surface, from which TMPA was extracted for each buffer, establishing one-to-one correspondence between the TMPA and rain gauge data (Yin et al. 2008).

Correction factors, including location and terrain variables, were determined for each buffer so that precipitation could be corrected with the aid of the topographic features. The location variables referred to longitude and latitude of the rain gauge, and the terrain variables were factors such as elevation, relative relief, slope, and aspect for each buffer. These were extracted from the DEM using ArcGIS tools (Yin et al. 2008). In total, 21 factors were extracted (Table 2). Correlation between the correction factors and rain gauge precipitation was analyzed using Statistical Package for the Social Sciences (SPSS) statistical software. Factors with a significance level greater than 0.01 were retained for subsequent rotated principal component (RPC) analysis (Yin et al. 2008). Factors that had a similar effect on precipitation were classified as one RPC. RPC scores for each rain gauge were calculated to prepare for further correction.

TABLE 2. Terrain variable definitions and their descriptions.

Variable name	Description
minelev	Minimum elevation inside 25-km buffers
maxelev	Maximum elevation inside 25-km buffers
rangelev	Range of elevation inside 25-km buffers
meanelev	Mean elevation inside 25-km buffers
stdelev	Std dev of elevation inside 25-km buffers
meanslp	Mean slope angle inside 25-km buffers
meanhshd	Mean lighting condition inside 25-km buffers
sumelev	Sum of all elevation inside 25-km buffers
medelev	Median elevation inside 25-km buffers
min_h	Minimum relative relief inside 25-km buffers
max_h	Maximum relative relief inside 25-km buffers
mean_h	Mean relative relief inside 25-km buffers
std_h	Std dev of relative relief inside 25-km buffers
n1_asp	Proportion of area with north-facing slopes inside 25-km buffers
ne2_asp	Proportion of area with northeast-facing slopes inside 25-km buffers
e3_asp	Proportion of area with east-facing slopes inside 25-km buffers
se4_asp	Proportion of area with southeast-facing slopes inside 25-km buffers
s5_asp	Proportion of area with south-facing slopes inside 25-km buffers
sw6_asp	Proportion of area with southwest-facing slopes inside 25-km buffers
w7_asp	Proportion of area with west-facing slopes inside 25-km buffers
nw8_asp	Proportion of area with northwest-facing slopes inside 25-km buffers

2) STEPWISE REGRESSION APPROACH

Stepwise regression analysis was conducted using SPSS to establish a regression equation by taking monthly TMPA precipitation, location variables, and RPC scores as independent variables and monthly rain gauge precipitation as a dependent variable. The corrected precipitation could then be determined according to the equation with the given TMPA precipitation and correction

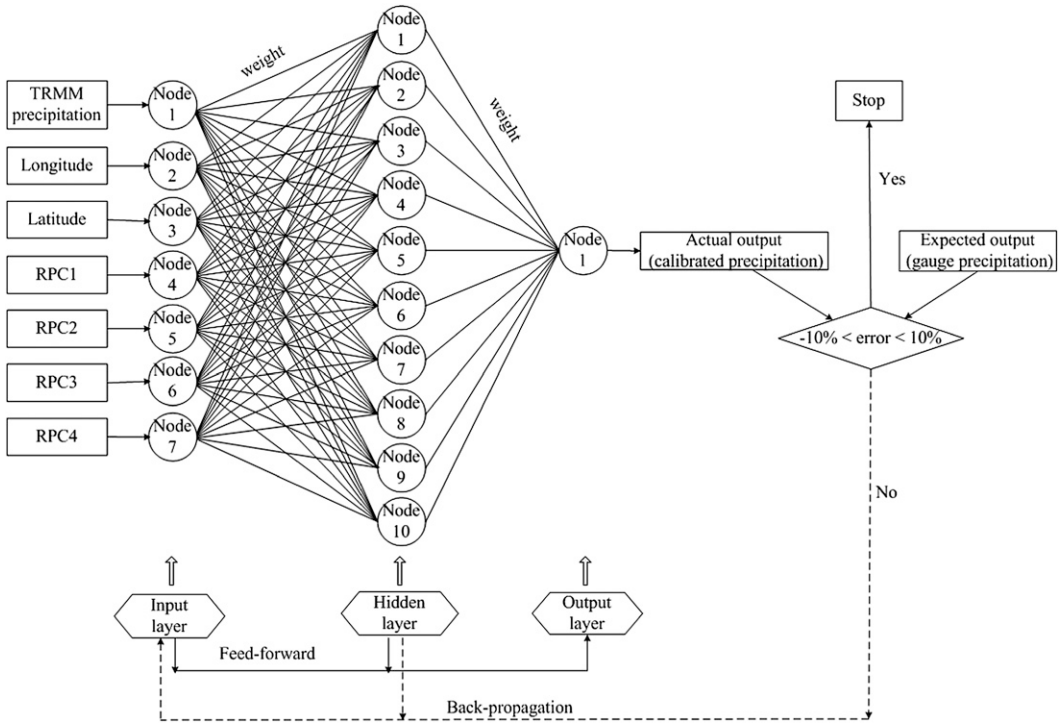

FIG. 2. Structure of the BP neural network.

factors (Yin et al. 2008). We considered stepwise regression a more reasonable method than the others mentioned in section 1 since it uses terrain variables as correction factors and may therefore be more applicable to our study area with complex topography. However, corrected TMPA precipitation was simply linearly summed by geolocation and topographic variables. Therefore, we tried the back-propagation (BP) neural network approach, which corrected TMPA data bias by including the correction factors nonlinearly.

3) BP NEURAL NETWORK APPROACH

The BP neural network approach was proposed by a scientific team led by Rumelhart and McCelland (1986) and has been widely used (Chang and Chao 2006; Moisen and Frescino 2002). The BP neural network structure contains three layers: input, hidden, and output (Fig. 2). Each layer contains at least one node. Nodes are connected by links, each of which represents a numerical weight.

The BP neural network algorithm consists of two procedures, feed forward of input signals and back propagation of errors. In the feed forward, variables enter the network from the input layer, are then processed by the hidden layer, and are finally transmitted to the output layer. In this process, previous node values and their specific weights were multiplied and followed by summing; the summation was then used as an input variable of activity function $\{y = 1/[1 + \exp(-x)]$; Chiang et al. 2006; Liu and Yang 2007; Wang et al. 2013$\}$ so that the current node value could be determined. In case the network error between the actual and expected output is unsatisfactory, the errors are used as adjusted signals and propagated from the output layer to the hidden layer and finally to the input layer. By doing this, weights between the nodes are adjusted to more reasonable values and error can be reduced (Wu and Li 2007). Feed forward and back propagation are repeated until the error between actual and expected output is reduced to within an acceptable range.

In this work, the BP neural network approach was realized in the matrix laboratory (MATLAB) environment. The network contained one input layer, one hidden layer, and one output layer, and each layer contained 7, 10, and 1 nodes, respectively. Monthly TMPA precipitation, location variables, and RPC scores were used as input variables. The expected output was rain gauge precipitation, and actual output of the BP neural network was bias-corrected TMPA precipitation. Seven input variables were processed by the hidden and output layers using the active function; therefore, corrected precipitation was not a simple linear combination of input variables. This was the most important improvement over the stepwise regression method.

4) INDICES FOR EVALUATING TMPA AND CORRECTED TMPA DATA

Original TMPA precipitation and that corrected by stepwise regression were evaluated on the basis of observed precipitation data. TMPA precipitation corrected by the BP neural network was compared with both observed precipitation data and results from stepwise regression for evaluating performance of that network approach.

The frequency bias index (FBI), probability of detection (POD), and false alarm ratio (FAR) were defined for evaluating precipitation occurrence (Barros et al. 2000; Su et al. 2008). Relative mean bias (bias), Nash–Sutcliffe efficiency (NSE), correlation coefficient (R^2), and determination coefficient of regression equation (r^2) were used to assess precipitation amount (Vila et al. 2009).

The FBI indicates any tendency to underestimate (FBI < 1) or overestimate (FBI > 1) precipitation occurrence, with 1 being a perfect estimate. POD indicates the fraction of precipitation occurrences that are correctly detected, again with 1 being a perfect value. The FAR measures the fraction of precipitation detections that are false alarms, with 0 being a perfect value. Overall differences of precipitation were measured by bias and R^2. TMPA precipitation is approximately equal to the gauge value if bias is between -10% and $+10\%$. Bias greater than $+10\%$ or lower than -10% means overestimated or underestimated precipitation, respectively (Islam 2009). The degree of linear correlation between the two sets of precipitation is measured by R^2; the higher the R^2, the higher the degree of correlation. There is significant correlation for R^2 greater than 0.7 (Condom et al. 2011). NSE and r^2 measure strength of the linear relationship, with a perfect value being 1:

$$\mathrm{FBI} = \frac{a+b}{a+c}, \tag{1}$$

$$\mathrm{POD} = \frac{a}{a+c}, \tag{2}$$

$$\mathrm{FAR} = \frac{b}{a+b}, \tag{3}$$

$$\mathrm{NSE} = 1 - \frac{\sum_{i=1}^{n} (O_i - P_i)^2}{\sum_{i=1}^{n} (O_i - \overline{O})^2}, \tag{4}$$

and

$$\mathrm{bias} = \frac{\sum_{i=1}^{n} (P_i - O_i)}{\sum_{i=1}^{n} O_i} \times 100\%, \tag{5}$$

where a is the number of hits, b is the number false alarms, c is the number misses, and d is the number of zeros. The variable O_i is observed monthly precipitation, P_i is TRMM monthly precipitation, and $\overline{O}$ is observed mean monthly precipitation.

3. Results

a. Performance of TMPA precipitation

Precipitation detective ability of TRMM 3B42 and TRMM 3B43 showed regional differences, as shown in Fig. 3. TRMM 3B42 underestimated precipitation occurrences, while FBIs in most buffers of TRMM 3B43 achieved optimal value in the north of the Tian Shan mountain range. Both TRMM 3B42 and TRMM 3B43 overestimated precipitation occurrences for the rest of the study area (Figs. 3a,b). The two precipitation products have the same FBI values on the northward slope of the Kunlun Mountains and Qilian Mountains; TRMM 3B43 gave better FBIs than TRMM 3B42 in the north of the Tian Shan, while TRMM 3B42 gave better FBIs for the rest of the regions (Fig. 3c). PODs of TRMM 3B42 were all higher than 0.85, with 27 buffers achieving optimal value, mainly distributed on the northward slope of the Kunlun Mountains and Qilian Mountains (Fig. 3d). There were no detection errors for TRMM 3B43, and all of the PODs achieved optimal value (not shown). The two precipitation products showed little difference about FARs, which valued from 0 to 0.54, and most buffers in the north of the Tian Shan achieved optimal value (Fig. 3e).

Biases of TRMM 3B42 and TRMM 3B43 were -58% to 498% and -30% to 674%, respectively, and both of them overestimated precipitation in most buffers, as shown in Figs. 3f and 3g. TRMM 3B43 gave a larger number of buffers in which biases achieved an acceptable range than that of TRMM 3B42, as well as number of buffers in which precipitation was overestimated. Biases higher than 10% and smaller than -10% averaged 55.4% and -30.7% for TRMM 3B42 and 73.6% and -19.2% for TRMM 3B43, respectively, which indicated that the overestimation degree of TRMM 3B43 was higher than that of TRMM 3B42 and vice versa for underestimation degree. Additionally, correlation coefficients of TRMM 3B43 were higher than those of TRMM 3B42, and there were 64 and 32 buffers in which precipitation was significantly correlated with observed values for TRMM 3B43 and TRMM 3B42, respectively.

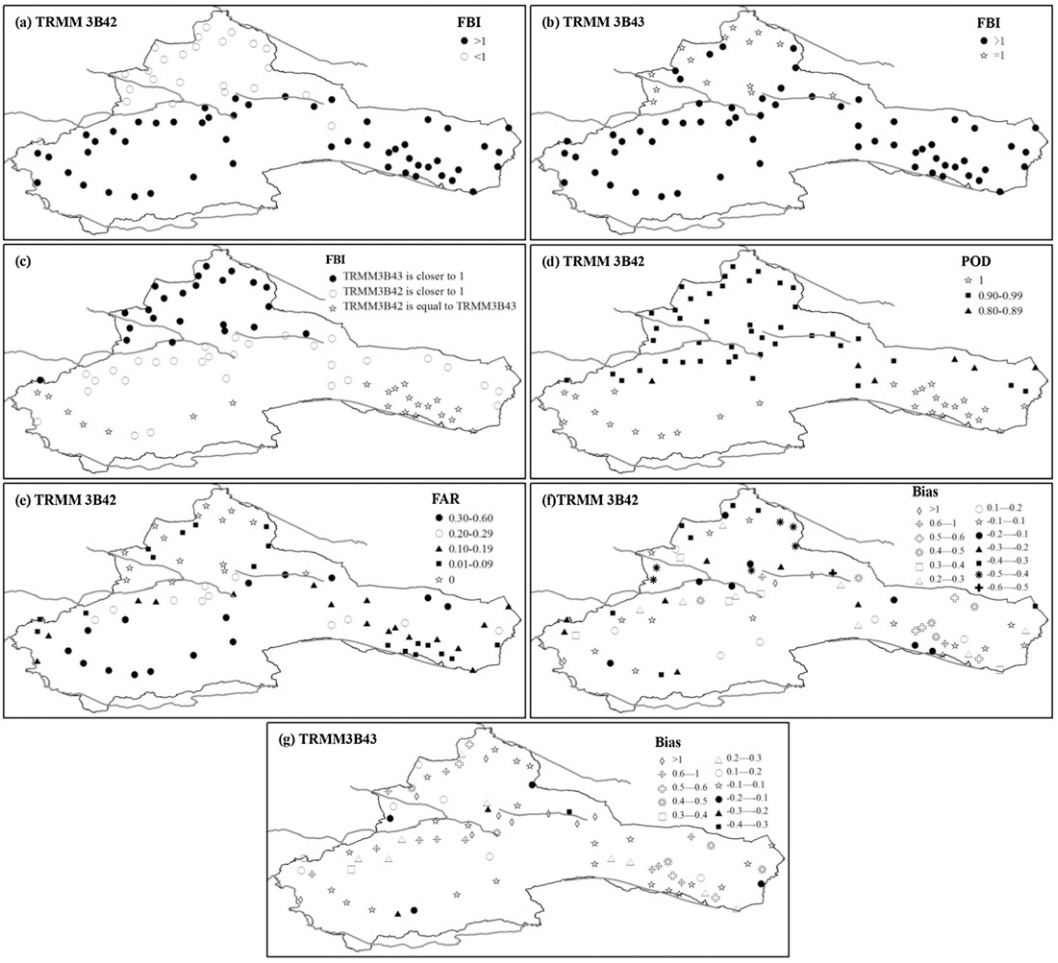

FIG. 3. Distribution of evaluating indices for original TMPA precipitation: (a) FBI of TRMM 3B42, (b) FBI of TRMM 3B43, (c) FBI comparison between TRMM 3B42 and TRMM 3B43, (d) POD of TRMM 3B42, (e) FAR of TRMM 3B42, (f) bias of TRMM 3B42, and (g) bias of TRMM 3B43.

The above analysis showed that both TRMM 3B42 and TRMM 3B43 overestimated precipitation occurrences and amounts in most buffers, and both of them gave a large proportion of false alarms. TRMM 3B43 gave better PODs, higher correlation coefficients, and lower underestimation degrees than TRMM 3B42, but it also gave higher overestimation degrees.

On the other hand, correlation coefficients were 0.35 to 0.75 and 0.71 to 0.84, NSEs were −0.31 to 0.53 and 0.01 to 0.70, and determination coefficients were −0.06 to 0.53 and 0.40 to 0.63 from January to December for TRMM 3B42 and TRMM 3B43, respectively. There are only two months (July and September) in which TRMM 3B42 was significantly correlated with observed precipitation, and NSEs were higher than 0.5. Comparatively, TRMM 3B43 gave a better performance because correlation coefficients were all higher than 0.7, NSEs were higher than 0.5 from June to October, and determination coefficients were higher than TRMM 3B42, except in February. However, biases for TRMM 3B42 were acceptable in 6 months (January, June–September, and December), while biases for TRMM 3B43 were higher than 10% and overestimated precipitation for all months.

Combining the above two aspects, overall, two TMPA products tended to overestimate precipitation in most cases and could not be fully accepted. Besides the limitations mentioned in section 1, there are some other causes for the unsatisfactory performance and overestimation of TMPA. The environmental condition is very important in the study area; perennial and seasonal snow–ice cover in the study area could be misclassified as rain clouds by passive microwave sensors (Hirpa et al. 2010), which may result in false alarms and precipitation overestimation. Also, a fraction of precipitation evaporates before it reaches the ground (Ferraro et al. 1998; McCollum et al. 2002; Rozante and Cavalcanti 2008),

TABLE 3. Results of rotated principal component analysis.

RPCs	RPC1		RPC2		RPC3		RPC4	
Eigenvalues	8.616		4.303		2.571		2.191	
	Variable	Loading value	Variable	Loading value	Variable	Loading value	Variable	Loading value
Represented variables	min_h	0.979	stdelev	0.91	s5_asp	0.786	w7_asp	−0.8
	minelev	0.978	std_h	0.91	sw6_asp	0.671	e3_asp	0.7
	meanhshd	0.957	rangelev	0.89	se4_asp	0.647		
	medelev	0.955	meanslp	0.81	ne2_asp	−0.69		
	meanelev	0.945			n1_asp	−0.85		
	mean_h	0.945						
	sumelev	0.922						
	max_h	0.822						
	maxelev	0.813						

which may cause overestimation. In addition, the evaluation results showed that TRMM 3B43 performed better than TRMM 3B42, although TRMM 3B43 showed a larger bias. In fact, the algorithms between TRMM 3B42 and TRMM 3B43 are very similar; the difference is that there is a certain amount of spatial smoothing in the 3B43-to-3B42 ratios. More seriously, there are limits on the ratios, approximately 0.2–3, so that large mismatches do not do too much damage to the histogram of 3B42 precipitation rates, and the ratios limitations may cause difference between accumulated TRMM 3B42 in a month and corresponding monthly TRMM 3B43. (G. J. Huffman 2013, personal communication). From this perspective, TRMM 3B43 performed better than TRMM 3B42, and

TABLE 4. Results of stepwise regression analysis for TRMM 3B42 and TRMM 3B43.

	TRMM 3B42								
Month	Constant	TRMM precipitation (mm)	Lon (°E)	Lat (°N)	RPC1	RPC2	RPC3	RPC4	r^2
Jan	−42.68	0.44		1.09		−0.71	−0.59	−0.67	0.30
Feb	−28.11	0.40		0.71		−0.46	−0.56	−0.59	0.40
Mar	−46.48	0.44		1.21	0.81		−1.13		0.23
Apr	−50.91	0.65		1.35			−1.13	−0.93	0.29
May	−48.94	0.58		1.38	3.70	2.18			0.36
Jun	0.53	0.71	−0.39	0.99	5.91	3.25		−1.72	0.57
Jul	−12.92	0.80	−0.26	1.04	9.68	5.48		−2.43	0.63
Aug	−33.59	0.71	−0.21	1.43	8.89	4.48			0.61
Sep	−9.56	0.74		0.36	3.63	3.10			0.60
Oct	−25.05	0.67	−0.08	0.86	0.85			−0.87	0.33
Nov	−67.98	0.51	−0.11	1.96	0.83	−1.42	−1.16	−1.30	0.40
Dec	−43.76	0.31	−0.07	1.28		−0.60	−0.98	−1.04	0.36
	TRMM 3B43								
Month	Constant	TRMM precipitation (mm)	Lon (°E)	Lat (°N)	RPC1	RPC2	RPC3	RPC4	r^2
Jan	−7.95	0.66	0.09		−0.71	−0.41		−0.76	0.63
Feb	−16.53	0.53		0.40		−0.56	−0.61	−0.66	0.56
Mar	−14.07	0.68	0.05	0.24			−1.06	−0.65	0.60
Apr	−8.03	0.85	0.08		−0.72		−1.13	−0.79	0.62
May	−18.10	0.85		0.44	1.66		−1.79	−1.11	0.63
Jun	23.85	0.83	−0.26		1.96	2.70	−1.01	−1.40	0.69
Jul	−0.04	0.89			5.13	4.65		−1.80	0.74
Aug	−1.40	0.87	−0.15	0.37	4.97	3.30		−1.13	0.75
Sep	0.38	0.89			1.85	2.35			0.72
Oct	0.12	0.81						−0.80	0.61
Nov	−14.39	0.67		0.35		−1.11	−0.71	−1.17	0.67
Dec	−5.56	0.68	0.06		−0.61		−0.64	−0.83	0.68

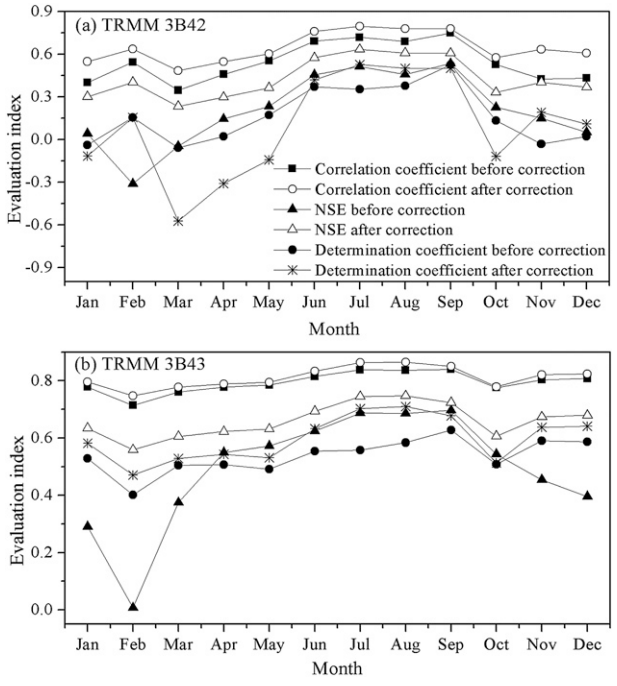

FIG. 4. Evaluation index before and after correction by the stepwise regression method.

the main reason may be due to the time scale, because finescale precipitation estimates tend to have high uncertainty (Huffman et al. 2007, 2010).

b. Correction of TMPA precipitation based on stepwise regression

Terrain variables were extracted from the DEM, then correlation analysis was performed, followed by principal component analysis, to prepare for calibration of TMPA precipitation via stepwise regression. The correlation analysis showed that terrain variables had significant correlation (at the 0.01 level) with precipitation for at least 1month, except for nw8_asp. Twenty factors remained to perform subsequent RPC analysis. Four RPCs were determined (Table 3), which explained more than 88% of variance of the original dataset. Each RPC represented at least one original terrain variable. Stepwise regression analysis was done using monthly TMPA precipitation, location variables, and RPC scores as independent variables and observed monthly precipitation as a dependent variable. Variables significant at the 0.05 level were allowed to enter the regression models.

The results showed that determination coefficients of regression models for TRMM 3B42 were relatively low from October to April (0.23–0.4) and got higher from May to September (0.57–0.63), as shown in Table 4a. The coefficients for TRMM 3B43 were ranged from 0.56 to 0.75 and higher than TRMM 3B42 for all months (Table 4b), which indicated that regression models for TRMM 3B43 were more reliable than TRMM 3B42.

Corrected TMPA precipitation was compared with rain gauge values to further assess method effectiveness (Fig. 4). The correlation coefficients and NSEs for corrected TRMM 3B42 increased by 0.03–0.21 and 0.07–0.71, respectively. There were 4 months (June–September) in which corrected precipitation was significantly related to observed value and NSEs were higher than 0.5. However, determination coefficients decreased in 6 months and were negative in 5 months. Comparatively, corrected TRMM 3B43 showed better improvement. The correlation coefficients were all higher than 0.75, although they showed only a little increment (0–0.03). NSEs were also increased for all months and were higher than 0.56. The determination coefficients ranged from 0.47 to 0.71 and higher than 0.6 in 6 months.

The above information indicates that corrected TMPA precipitation was superior to original data overall, which shows that stepwise regression method could improve TMPA data, especially for TRMM 3B43. However, the correction results for TRMM 3B42 were less effective, and the evaluation indices were too small to reach acceptable ranges for most months. In addition, negative corrected values existed in most months (not shown), and most negative values appeared from November through February, which accounts for 0%–19% and 2.9%–15.4% in total corrected values for TRMM 3B42 and TRMM 3B43, respectively. It was obvious that negative precipitation was contrary to the actual situation.

c. Correction of TMPA precipitation based on BP neural network

The stepwise regression method was followed by the BP neural network method to correct TMPA precipitation. The results showed that correlation coefficients between observed and corrected precipitation were 0.68–0.87 and 0.88–0.96, NSEs were 0.46–0.76 and 0.77–0.91, and determination coefficients were 0.29–0.73 and 0.74–0.91 for TRMM 3B42 and TRMM 3B43, respectively. Compared to the results of the stepwise regression method, the above three indices were all improved; they increased by 0.07–0.22 and 0.05–0.17, 0.1–0.32 and 0.09–0.29, and 0.19–0.86 and 0.12–0.36 for TRMM 3B42 and TRMM 3B43, respectively. In general, the corrected precipitation based on the BP neural network was closer to observed precipitation than that based on stepwise regression, indicating that a nonlinear model was more effective than a linear model.

After correction by a BP neural network, the scatters between observed and corrected precipitation were closer to the 1:1 line for both TRMM 3B42 and TRMM 3B43, as shown in Fig. 5. Corrected TRMM 3B43 was

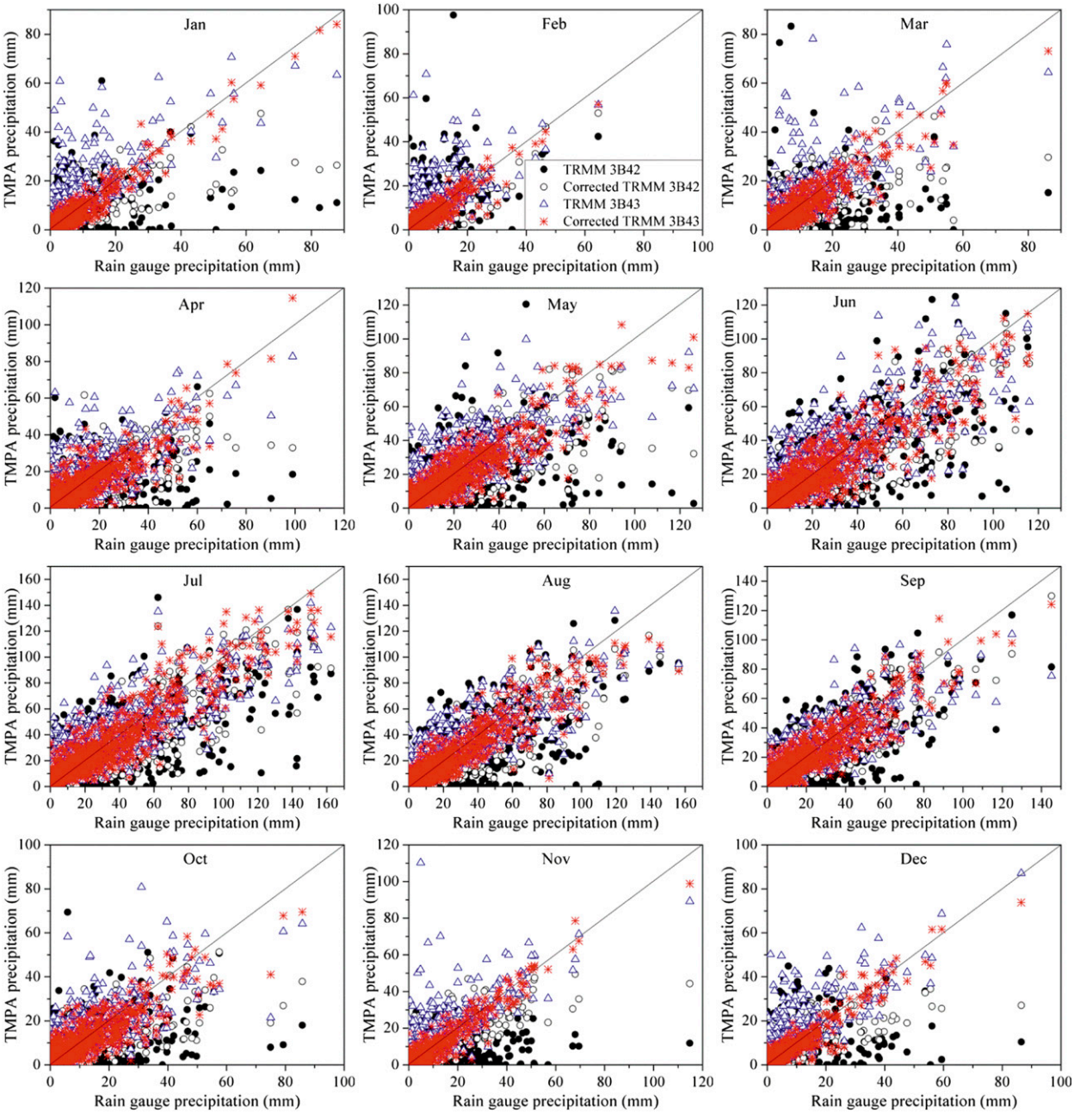

FIG. 5. Scatterplot of rain gauge and TMPA precipitation before and after correction based on the BP neural network for every month (on the scale of the entire study area).

significantly correlated with the observed value for all months, and biases ranged from −7.6% to 0.7%, as shown in Fig. 6, which indicated that corrected TRMM 3B43 could be accepted. However, determination coefficients of corrected TRMM 3B42 were still less than 0.5 for January, March, April, and October. Correlation coefficient and NSE in March were smaller than 0.7 and 0.5, respectively. In addition, biases were still higher than 10%, and precipitation was therefore overestimated in July and August, indicating that corrected TRMM 3B42 was still unsatisfactory in a few months.

From the results of the stepwise regression and the BP neural network, it is obvious that both of them had better correction for TRMM 3B43 than TRMM 3B42. It has been shown previously that TRMM 3B43 had better linear correlation with observed precipitation, but biases

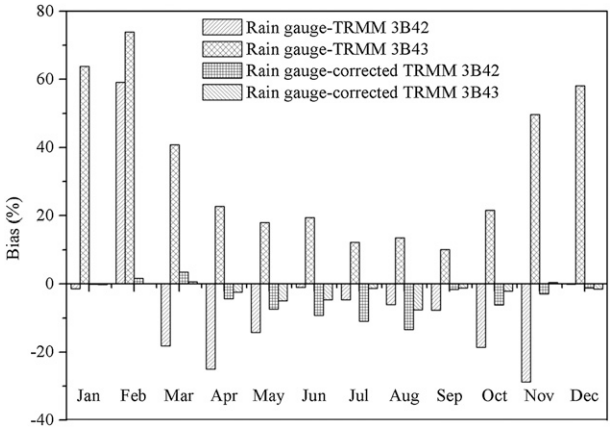

FIG. 6. Biases between rain gauge and TMPA precipitation before and after correction based on the BP neural network for every month.

were higher than TRMM 3B42 and it could be inferred that correction results were affected more by linear correlation degree than the biases of the original data.

d. Spatial-scale dependence of correction methods

The aforementioned results were for the entire study area, and TMPA precipitation was also corrected on a subregion scale by the two methods. Figure 7 shows that the precipitation in subregions was significantly improved after correction and scatters were closer to the 1:1 line. Compared with correction over the entire area, correlation coefficients of subregions increased by 0.01–0.23 and 0.01–0.22 for TRMM 3B42 and TRMM3B43, respectively, and corrected precipitation was significantly related to observed precipitation, except for subregions 1 and 5, which were corrected by stepwise regression method. Biases ranged from −7.28% to 0.06% and −5.6% to 0.4%, decreasing by 122.9%–6.7% and 0.6%–79.8% for TRMM 3B42 and TRMM3B43, respectively. This reveals that correction on the subregion scale was more accurate than on the larger scale. TRMM 3B43 corrected by the two methods on the subregion scale was acceptable for every subregion, as well as TRMM 3B42 corrected by the BP neural network method. Additionally, the BP neural network method showed higher correlations and biases than stepwise regression; however, negative corrected precipitation by the latter method may be responsible for the lower biases.

4. Discussion

Rain gauges are the most direct method to measure near-surface precipitation, and rain gauge observations yield relatively accurate point measurements of precipitation, but they also suffer from sampling error in representing area means (Xie and Arkin 1995). In this study, rain gauge precipitation was treated as the true value in the buffer of 25 km in diameter centered at the rain gauge. Generally speaking, there should be more than enough rain gauges in a region to make sure that the average precipitation is representative of that region. Xie and Arkin (1995) indicated that at least five gauges are needed to produce a good average monthly precipitation for grid areas of 2.5° × 2.5° with an accuracy of 10%, but only 10% of the global land grid areas satisfy this requirement. Limited by sparse rain gauges, some previous studies treated the point rain gauge observation as the truth in 0.25° or 1° pixels over complex terrain. For example, Yin et al. (2008) corrected a 1° × 1° TRMM 3B42 version 5 product by taking a single rain gauge precipitation as the actual value in the buffer of 50 km over the Tibetan Plateau. Hirpa et al. (2010) evaluated TRMM 3B42RT, CMORPH, and PERSIANN with rain gauge precipitation over very complex terrain in Ethiopia and took a single rain gauge precipitation as the true value in 0.25° pixel. Tobin and Bennett (2010) compared and adjusted five 0.25° grids of the TMPA research product that corresponds with the Douglas rain gauge in the San Pedro River basin (1971 km^2). Similar examples can also be found in Islam (2009) and Heidinger et al. (2012). To further interpret whether the point rain gauge observation could be treated as the truth in the buffer of 25 km, we extracted terrain factors (listed in Table 2) in a series of buffers with different sizes centered at every rain gauge (5, 10, 15, 20, 25, 30, 35, and 40 km in diameter). Correlation coefficients were calculated between rain gauge precipitation and terrain factors in every buffer, followed by a significance test between correlation coefficients of adjacent buffers. The results showed that there were no significant differences (sig) between buffers of 5 and 10 km (sig = 0.781), 10 and 15 km (sig = 0.908), 15 and 20 km (sig = 0.409), 20 and 25 km (sig = 0.051), and 25 and 30 km (sig = 0.904). However, correlation coefficients between buffers of 30 and 35 km (sig = 0.001) and 35 and 40 km (sig = 0.001) were significantly different. This result indicates that the terrain factors have similar influence on the precipitation in a 30-km area centered at a rain gauge, and the precipitation could be treated homogeneously in this area. Thus, a buffer size of 25 km can be accepted.

Satellite precipitation has error and bias from indirect observation and uncertainty in the precipitation retrieval algorithm, especially for high-latitude or mountain areas. Many efforts have been made to correct this precipitation, and most were statistically based (Tian et al. 2010; Tobin and Bennett 2010), only considering probabilistic relationships between rain gauge and satellite precipitation. However, the performance of satellite

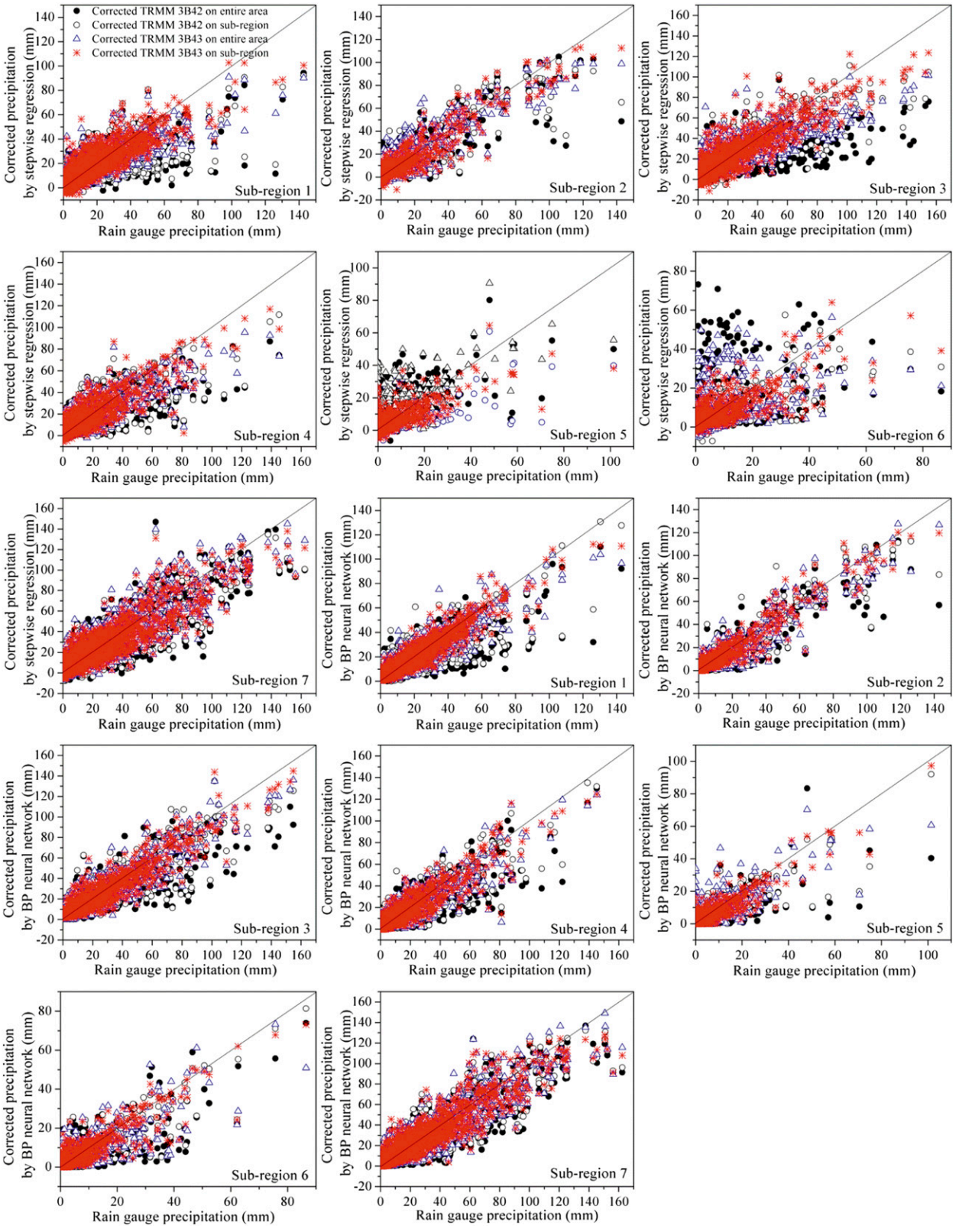

FIG. 7. Scatterplot of rain gauge and TMPA precipitation before and after correction using stepwise regression and the BP neural network for every subregion.

precipitation was affected by many factors (e.g., local topography), and the aforementioned methods may be not applicable to the areas of complex terrain. Correcting TRMM precipitation using the stepwise regression proposed by Yin et al. (2008) achieved satisfactory results for the Tibetan Plateau. This type of method was more applicable because it considered terrain variables as correcting factors. However, negative values appeared in the regression results for our study area. Moreover, consistency between corrected and rain gauge precipitation was not satisfactory. The results of the BP neural network showed greater consistency between corrected and rain gauge precipitation than those of stepwise regression. Bode (2000) indicated that the artificial neural network was more precise than traditional linear regression and nonlinear regression methods in cost estimation, and our results showed that the BP method was more applicable in correcting precipitation. Terrain variables and precipitation in the study area may not be simply described by linear relationship; conversely, nonlinearity showed better efficiency.

Parameters such as the number of hidden layers and their nodes and learning rate affect the BP neural network effectiveness (Ju et al. 2009). The numbers of hidden layers and nodes increase network complexity. Convergence speed is too slow when the learning rate is small, and error will vary greatly if that rate is too high. In this study, we adjusted all these parameters; the output changed slightly, and error could not be reduced by further parameter change. The ultimate parameters were set when the correction achieved best results: one hidden layer with 10 nodes was adopted and the learning rate was 0.01. Earlier study showed that input data should be processed more efficiently to enhance prediction accuracy (Ju et al. 2009). However, the original TMPA precipitation as an input variable gave unpleasant precision in the study area. Therefore, accuracy of corrected precipitation was limited by the quality of input TMPA precipitation.

5. Conclusions

In this study, two TMPA precipitation products (TRMM 3B42 and TRMM 3B43) during 1998–2010 were evaluated and corrected in the arid area of northwest China. TMPA showed unsatisfactory performance and precision since it overestimated precipitation occurrence and amount in most cases, as well as producing numerous false alarms. Corrected TMPA precipitation based on stepwise regression was closer to observed values, but the results remained unsatisfactory. The BP neural network, which was a nonlinear model, showed better correction results than traditional linear regression approaches. Both correction methods were affected by region size and were more effective on a smaller spatial scale than over the entire study area. However, the BP method was limited by the poor quality of the original TMPA precipitation. In addition, both methods gave better correction results for TRMM 3B43 than for TRMM 3B42. TRMM 3B43 results corrected regionally by stepwise regression and corrected both regionally and nonregionally by the BP neural network were acceptable, but satisfactory results were only found in TRMM 3B42 corrected regionally by the BP neural network.

Acknowledgments. This study is supported partially by the 973 Program of China (Grant 2010CB951002), Natural Science Foundation of China (Grant 41130641), and the Project of the National Eleventh Five-Year Research Program of China (Grant 2012BAC19B07).

REFERENCES

Barros, A. P., M. Joshi, J. Putkonen, and D. W. Burbank, 2000: A study of the 1999 monsoon rainfall in a mountainous region in central Nepal using TRMM products and rain gauge observations. *Geophys. Res. Lett.,* **27,** 3683–3686, doi:10.1029/2000GL011827.

——, S. Chiao, T. J. Lang, D. Burbank, and J. Putkonen, 2006: From weather to climate—Seasonal and interannual variability of storms and implications for erosion processes in the Himalaya. *Tectonics, Climate, and Landscape Evolution,* S. D. Willett et al., Eds., Geological Society of America Special Paper, No. 398, Geological Society of America, 17–38.

Bode, J., 2000: Neural networks for cost estimation: Simulations and pilot application. *Int. J. Prod. Res.,* **38,** 1231–1254, doi:10.1080/002075400188825.

Boushaki, F. I., K. L. Hsu, S. Sorooshian, G. H. Park, S. Mahani, and W. Shi, 2009: Bias adjustment of satellite precipitation estimation using ground-based measurement: A case study evaluation over the southwestern United States. *J. Hydrometeor.,* **10,** 1231–1242, doi:10.1175/2009JHM1099.1.

Bowman, K. P., 2005: Comparison of TRMM precipitation retrievals with rain gauge data from ocean buoys. *J. Climate,* **18,** 178–190, doi:10.1175/JCLI3259.1.

Chang, T. C., and R. J. Chao, 2006: Application of back-propagation networks in debris flow prediction. *Eng. Geol.,* **85,** 270–280, doi:10.1016/j.enggeo.2006.02.007.

Chen, X., B. L. Li, Q. Li, J. L. Li, and S. Abdulla, 2012: Spatiotemporal pattern and changes of evapotranspiration in arid central Asia and Xinjiang of China. *J. Arid Land,* **4,** 105–112, doi:10.3724/SP.J.1227.2012.00105.

Chiang, W. K., D. S. Zhang, and L. Zhou, 2006: Predicting and explaining patronage behavior toward web and traditional stores using neural networks: A comparative analysis with logistic regression. *Decis. Support Syst.,* **41,** 514–531, doi:10.1016/j.dss.2004.08.016.

Cohen Liechti, T., J. P. Matos, J. L. Boillat, and A. J. Schleiss, 2012: Comparison and evaluation of satellite derived precipitation products for hydrological modeling of the Zambezi River basin. *Hydrol. Earth Syst. Sci.,* **16,** 489–500, doi:10.5194/hess-16-489-2012.

Collischonn, B., W. Collischonn, and C. E. M. Tucci, 2008: Daily hydrological modeling in the Amazon basin using TRMM rainfall estimates. *J. Hydrol.,* **360,** 207–216, doi:10.1016/j.jhydrol.2008.07.032.

Condom, T., P. Rau, and J. C. Espinoza, 2011: Correction of TRMM 3B43 monthly precipitation data over the mountainous areas of Peru during the period 1998–2007. *Hydrol. Processes,* **25,** 1924–1933, doi:10.1002/hyp.7949.

Dinku, T., P. Ceccato, E. Grover-Kopec, M. Lemma, S. Connor, and C. Ropelewski, 2007: Validation of satellite rainfall products over East Africa's complex topography. *Int. J. Remote Sens.,* **28,** 1503–1526, doi:10.1080/01431160600954688.

——, S. Chidzambwa, P. Ceccato, S. J. Connor, and C. F. Ropelewski, 2008: Validation of high-resolution satellite rainfall products over complex terrain. *Int. J. Remote Sens.,* **29,** 4097–4110, doi:10.1080/01431160701772526.

Duncan, M. R., B. Austin, F. Fabry, and G. L. Austin, 1993: The effect of gauge sampling density on the accuracy of streamflow prediction for rural catchments. *J. Hydrol.,* **142,** 445–476, doi:10.1016/0022-1694(93)90023-3.

Ebert, E. E., J. E. Janowiak, and C. Kidd, 2007: Comparison of near-real-time precipitation estimates from satellite observations and numerical models. *Bull. Amer. Meteor. Soc.,* **88,** 47–64, doi:10.1175/BAMS-88-1-47.

Ferraro, R. R., E. A. Smith, W. Berg, and G. J. Huffman, 1998: A screening methodology for passive microwave precipitation retrieval algorithms. *J. Atmos. Sci.,* **55,** 1583–1600, doi:10.1175/1520-0469(1998)055<1583:ASMFPM>2.0.CO;2.

Gan, T. Y., E. M. Dlamini, and G. F. Biftu, 1997: Effects of model complexity and structure, data quality, and objective functions on hydrologic modeling. *J. Hydrol.,* **192,** 81–103, doi:10.1016/S0022-1694(96)03114-9.

Heidinger, H., C. Yarlequé, A. Posadas, and R. Quiroz, 2012: TRMM rainfall correction over the Andean Plateau using wavelet multi-resolution analysis. *Int. J. Remote Sens.,* **33,** 4583–4602, doi:10.1080/01431161.2011.652315.

Hirpa, F. A., M. Gebremichael, and T. Hopson, 2010: Evaluation of high-resolution satellite precipitation products over very complex terrain in Ethiopia. *J. Appl. Meteor. Climatol.,* **49,** 1044–1051, doi:10.1175/2009JAMC2298.1.

Hong, Y., D. Gochis, J. Cheng, K. Hsu, and S. Sorooshian, 2007: Evaluation of PERSIANN-CCS rainfall measurement using the NAME Event Rain Gauge Network. *J. Hydrometeor.,* **8,** 469–482, doi:10.1175/JHM574.1.

Huffman, G. J., and D. T. Bolvin, 2013: TRMM and other data precipitation data set documentation. Mesoscale Atmospheric Processes Laboratory, NASA Goddard Space Flight Center and Science Systems and Applications, Inc., 40 pp.

——, R. F. Adler, E. Stocker, D. T. Bolvin, and E. J. Nelkin, 2003: Analysis of TRMM 3-hourly multi-satellite precipitation estimates computed in both real and post-real time. Preprints, *12th Conf. on Satellite Meteorology and Oceanography,* Long Beach, CA, Amer. Meteor. Soc., P4.11. [Available online at https://ams.confex.com/ams/pdfpapers/54906.pdf.]

——, and Coauthors, 2007: The TRMM multisatellite precipitation analysis (TMPA): Quasi-global, multiyear, combined-sensor precipitation estimates at fine scales. *J. Hydrometeor.,* **8,** 38–55, doi:10.1175/JHM560.1.

——, R. F. Adler, D. T. Bolvin, and E. J. Nelkin, 2010: The TRMM Multi-Satellite Precipitation Analysis (TMPA). *Satellite Rainfall Applications for Surface Hydrology,* M. Gebremichael and F. Hossain, Eds., Springer, 3–22.

Islam, M. N., 2009: Analysis of TRMM data in monitoring rainfall over mountainous regions. SMRC Rep. 27, SAARC Meteorological Research Centre (SMRC), Dhaka, Bangladesh, 48 pp.

Janowiak, J., R. Joyce, and P. P. Xie, 2009: CMORPH improvements: A Kalman filter approach to blend various satellite rainfall estimate inputs and rain gauge data integration. *Extended Abstracts, EGU General Assembly 2009,* Vienna, Austria, European Geophysical Union, 9810. [Available online at http://meetingorganizer.copernicus.org/EGU2009/EGU2009-9810.pdf.]

Joyce, R. J., J. E. Janowiak, P. A. Arkin, and P. Xie, 2004: CMORPH: A method that produces global precipitation estimates from passive microwave and infrared data at high spatial and temporal resolution. *J. Hydrometeor.,* **5,** 487–503, doi:10.1175/1525-7541(2004)005<0487:CAMTPG>2.0.CO;2.

Ju, Q., Z. B. Yu, Z. C. Hao, G. X. Ou, J. Zhao, and D. D. Liu, 2009: Division-based rainfall-runoff simulations with BP neural networks and Xinanjiang model. *Neurocomputing,* **72,** 2873–2883, doi:10.1016/j.neucom.2008.12.032.

Karaseva, M. O., S. Prakash, and R. Gairola, 2012: Validation of high-resolution TRMM-3B43 precipitation product using rain gauge measurements over Kyrgyzstan. *Theor. Appl. Climatol.,* **108,** 147–157, doi:10.1007/s00704-011-0509-6.

Kummerow, C., 1998: Beamfilling errors in passive microwave rainfall retrievals. *J. Appl. Meteor.,* **37,** 356–370, doi:10.1175/1520-0450(1998)037<0356:BEIPMR>2.0.CO;2.

Li, M., and Q. X. Shao, 2010: An improved statistical approach to merge satellite rainfall estimates and raingauge data. *J. Hydrol.,* **385,** 51–64, doi:10.1016/j.jhydrol.2010.01.023.

Liu, C. L., and T. Y. Yang, 2007: Study on method of GPS height fitting based on BP artificial neural network. *J. Southwest Jiaotong Univ.,* **2,** 5.

Mätzler, C., and A. Standley, 2000: Technical note: Relief effects for passive microwave remote sensing. *Int. J. Remote Sens.,* **21,** 2403–2412, doi:10.1080/01431160050030538.

McCollum, J. R., W. F. Krajewski, R. R. Ferraro, and M. B. Ba, 2002: Evaluation of biases of satellite rainfall estimation algorithms over the continental United States. *J. Appl. Meteor.,* **41,** 1065–1080, doi:10.1175/1520-0450(2002)041<1065:EOBOSR>2.0.CO;2.

Moisen, G. G., and T. S. Frescino, 2002: Comparing five modelling techniques for predicting forest characteristics. *Ecol. Modell.,* **157,** 209–225, doi:10.1016/S0304-3800(02)00197-7.

Morrissey, M. L., and J. S. Greene, 1993: Comparison of two satellite-based rainfall algorithms using Pacific atoll raingage data. *J. Appl. Meteor.,* **32,** 411–425, doi:10.1175/1520-0450(1993)032<0411:COTSBR>2.0.CO;2.

Nicholson, S. E., and Coauthors, 2003b: Validation of TRMM and other rainfall estimates with a high-density gauge dataset for West Africa. Part II: Validation of TRMM rainfall products. *J. Appl. Meteor.,* **42,** 1355–1368, doi:10.1175/1520-0450(2003)042<1355:VOTAOR>2.0.CO;2.

Rozante, J. R., and I. Cavalcanti, 2008: Regional Eta model experiments: SALLJEX and MCS development. *J. Geophys. Res.,* **113,** D17106, doi:10.1029/2007JD009566.

Rumelhart, D. E., and J. L. McCelland, 1986: *Parallel Distributed Processing.* MIT Press, 317 pp.

Scheel, M., M. Rohrer, C. Huggel, D. Santos Villar, E. Silvestre, and G. Huffman, 2010: Evaluation of TRMM Multi-satellite Precipitation Analysis (TMPA) performance in the central Andes region and its dependency on spatial and temporal resolution. *Hydrol. Earth Syst. Sci. Discuss.,* **7,** 8545–8586, doi:10.5194/hessd-7-8545-2010.

Shi, Y. F., Y. P. Shen, E. Kang, D. L. Li, Y. J. Ding, G. W. Zhang, and R. J. Hu, 2007: Recent and future climate change in northwest China. *Climatic Change,* **80,** 379–393, doi:10.1007/s10584-006-9121-7.

Sorooshian, S., K. L. Hsu, X. G. Gao, H. V. Gupta, B. Imam, and D. Braithwaite, 2000: Evaluation of PERSIANN system satellite-based estimates of tropical rainfall. *Bull. Amer. Meteor. Soc.,* **81,** 2035–2046, doi:10.1175/1520-0477(2000)081<2035:EOPSSE>2.3.CO;2.

Su, F. G., Y. Hong, and D. P. Lettenmaier, 2008: Evaluation of TRMM Multisatellite Precipitation Analysis (TMPA) and its utility in hydrologic prediction in the La Plata Basin. *J. Hydrometeor.,* **9,** 622–640, doi:10.1175/2007JHM944.1.

Su, H. C., Y. P. Shen, P. Han, J. Li, and Y. C. Lan, 2007: Precipitation and its impact on water resources and ecological environment in Xinjiang region. *J. Glaciol. Geocryol.,* **29,** 343–350.

Tian, Y. D., C. D. Peters-Lidard, R. F. Adler, T. Kubota, and T. Ushio, 2010: Evaluation of GSMaP precipitation estimates over the contiguous United States. *J. Hydrometeor.,* **11,** 566–574, doi:10.1175/2009JHM1190.1.

Tobin, K. J., and M. E. Bennett, 2010: Adjusting satellite precipitation data to facilitate hydrologic modeling. *J. Hydrometeor.,* **11,** 966–978, doi:10.1175/2010JHM1206.1.

Vila, D. A., L. G. G. de Goncalves, D. L. Toll, and J. R. Rozante, 2009: Statistical evaluation of combined daily gauge observations and rainfall satellite estimates over continental South America. *J. Hydrometeor.,* **10,** 533–543, doi:10.1175/2008JHM1048.1.

Wang, H. S., Y. N. Wang, and Y. C. Wang, 2013: Cost estimation of plastic injection molding parts through integration of PSO and BP neural network. *Expert Syst. Appl.,* **40,** 418–428, doi:10.1016/j.eswa.2012.01.166.

Wu, J.-B., and W.-J. Li, 2007: Study on textile industry using BP neural networks. *Prog. Text. Sci. Technol.,* **2** (2), 7–10.

Xie, P. P., and P. A. Arkin, 1995: An intercomparison of gauge observations and satellite estimates of monthly precipitation. *J. Appl. Meteor.,* **34,** 1143–1160, doi:10.1175/1520-0450(1995)034<1143:AIOGOA>2.0.CO;2.

Yan, J., and M. Gebremichael, 2009: Estimating actual rainfall from satellite rainfall products. *Atmos. Res.,* **92,** 481–488, doi:10.1016/j.atmosres.2009.02.004.

Yin, Z. Y., X. D. Liu, X. Q. Zhang, and C. F. Chung, 2004: Using a geographic information system to improve Special Sensor Microwave Imager precipitation estimates over the Tibetan Plateau. *J. Geophys. Res.,* **109,** D03110, doi:10.1029/2003JD003749.

——, X. Zhang, X. Liu, M. Colella, and X. Chen, 2008: An assessment of the biases of satellite rainfall estimates over the Tibetan Plateau and correction methods based on topographic analysis. *J. Hydrometeor.,* **9,** 301–326, doi:10.1175/2007JHM903.1.

Zhang, Q., V. P. Singh, J. F. Li, F. Q. Jiang, and Y. G. Bai, 2012: Spatio-temporal variations of precipitation extremes in Xinjiang, China. *J. Hydrol.,* **434–435,** 7–18, doi:10.1016/j.jhydrol.2012.02.038.

Zhang, X. Q., Y. Sun, D. Zheng, and W. Y. Mao, 2011: Responses of temperature zone boundaries in the arid region of China to climatic warming. *Acta Geogr. Sin.,* **66,** 1166–1178.

Zhao, C. Y., F. Z. Shi, Y. Sheng, J. Li, Z. M. Zhao, M. Han, and Y. Yimamu, 2011: Regional differentiation characteristics of precipitation changing with altitude in Xinjiang region in recent 50 years. *J. Glaciol. Geocryol.,* **33,** 1203–1213.